Eur. Phys. J. D **4**, 139–144 (1998)

**THE EUROPEAN PHYSICAL JOURNAL D**



# Anisotropy of optical suppression in photoassociative ionization collisions within a slow, collimated sodium atom beam

C.-C. Tsao[a], Y. Wang, R. Napolitano[b], and J. Weiner[c]

Laboratory for Atomic, Molecular, and Optical Science and Engineering, University of Maryland, College Park, Maryland 20742, USA

Received: 8 January 1998 / Revised: 6 April 1998 / Accepted: 10 May 1998

**Abstract.** We report the observation of polarization anisotropy in the optical suppression of photoassociative ionization (PAI) collisions. Binary collisions occur within a tightly collimated and optically cooled velocity group of a single sodium beam. A laser beam, blue-detuned with respect to the atomic resonance transition, crosses the atomic beam and suppresses the PAI rate. We measure this suppression as a function of intensity and electric field vector aligned parallel or perpendicular to the atomic beam axis. Quantum close-coupling and multichannel curve-crossing calculations of model systems yield insight into the nature of the anisotropy and are in reasonable agreement with the measurements.

**PACS.** 32.80.Pj Optical cooling of atoms; trapping – 34.50.Rk Laser-modified scattering and reactions

## 1 Introduction

Manipulating atomic collisions by imposing optical fields of varying intensity, frequency, and polarization has been a theme of enduring interest in atomic, molecular, optical, and chemical physics. The development over the past fifteen years of atom cooling to submillikelvin temperatures and confinement in optical and magnetic traps has triggered a resurgence of interest in binary processes and has led to important advances in the precision spectroscopy of photoassociation collisions [1]. In addition to inducing these bond-forming inelastic collisions, optical fields can be used to suppress inelastic collision rates and shield atoms from close approach. Optical suppression of photoassociative ionization was first reported in experiments carried out in a sodium atom magneto-optic trap (MOT) [2]. Follow-up experiments on the power dependence [3] and polarization dependence (linear *vs.* circular) [4], revealed marked deviations from the predictions of simple one-dimensional, dressed-state curve-crossing models. In particular the suppression effect was found to be significantly less pronounced than predicted at high intensities and that circular polarization was a more effective suppressor than linear. Collisional ionization experiments in rare-gas MOTs showed similar suppression effects [5,6] with even more pronounced deviations from the predictions of simple 1D models [7]. The discord between experiment and theory motivated the development of a 3D quantum close-coupling model with a more exact treatment of high-power light-field coupling to the quasimolecule [8]. Application of this theory to the sodium MOT experiments showed much better agreement with the observed power dependence of the suppression effect and correctly predicted that circular polarization should be more effective than linear. These model calculations also revealed that optical shielding and suppression with linearly polarized light should exhibit an anisotropy with respect to the angle between the polarization and molecular axes: with increasing intensity, suppressor light polarized perpendicular should be more effective than light polarized parallel. Because the angular averaging of collision axes in a three-dimensional trap masks this polarization effect, we undertook to study optical suppression under conditions where the distribution of collision angles is greatly restricted. We report here therefore the first measurements of optical suppression of photoassociative ionization within a highly collimated, cooled atomic beam. These initial results indeed reveal a pronounced anisotropy in the suppression effect and are in good agreement with calculations obtained from the quantum close-coupling model [8] and a recently proposed multichannel curve crossing model [9].

## 2 Description of the experiment

Figure 1 shows a schematic layout of the apparatus. A conventional sodium vapor oven source furnishes a flux of sodium atoms that is collimated by a skimmer and injected into a tapered-solenoid Zeeman slower [10].

[a] *Present address*: Mail Code 127-72, California Institute of Technology, Pasadena, CA 91125, USA.

[b] *Present address*: Instituto de Física de São Carlos, Universidade de São Paulo, São Carlos, SP 13560, Brazil.

[c] *Also*: Université Paul Sabatier, IRSAMC/CAR, 118 route de Narbonne, 31062 Toulouse Cedex, France.
e-mail: `jweiner@annick2.umd.edu`

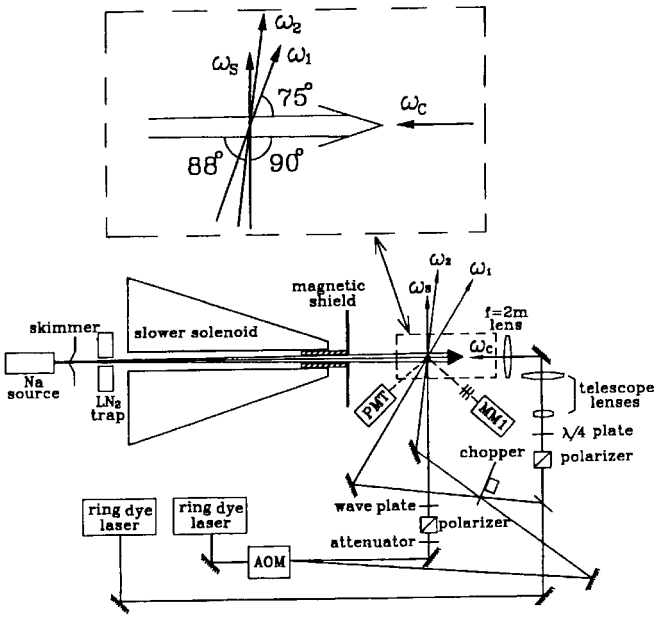


**Fig. 1.** Schematic diagram of the apparatus. Inset shows disposition of light beams used for axial cooling of the atom beam, $\omega_c$, induction of PAI, $\omega_1$, $\omega_2$, and the suppressor field, $\omega_s$.

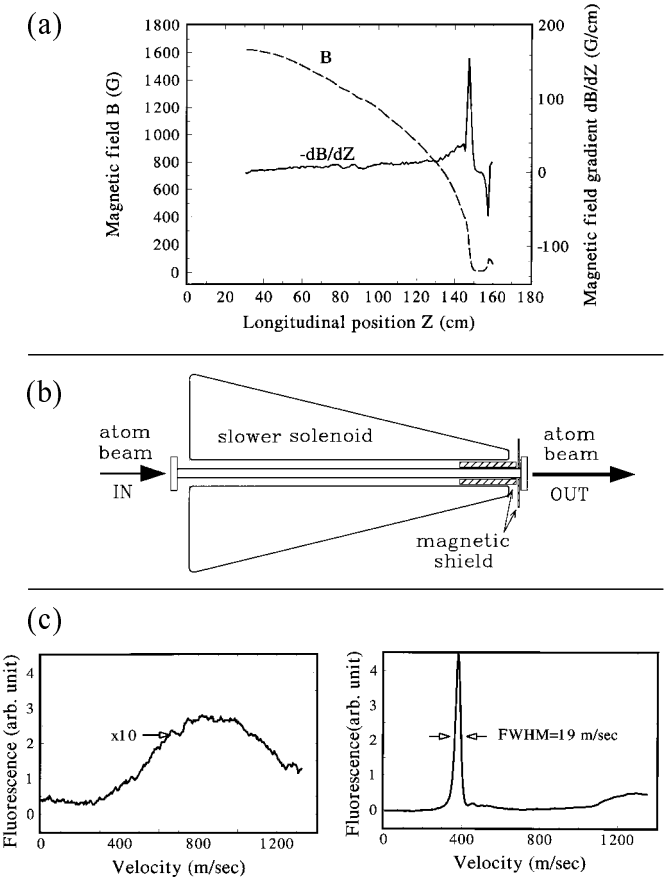


**Fig. 2.** (a) Magnetic field and gradient within the Zeeman slower. (b) Detail of the Zeeman slower showing the position of the magnetic shield. (c) Measured velocity distributions in the atom beam at the entrance and exit of the Zeeman slower.

An annular liquid nitrogen trap surrounding the atom beam and a small diffusion pump minimize background alkali vapor entering the deceleration tube by pumping away the skimmed-off atom flux. A single-mode light beam, $\omega_c$, coupled to the $^2S_{1/2}(F = 2) \rightarrow {}^2P_{3/2}(F' = 3)$ cycling transition and counterpropagating to the atom beam, decelerates and cools a fraction of the atom flux. Near the end of the Zeeman slower a small cylindrical fixture wrapped with 15 turns of $\mu$ metal foil (0.025 mm thick) is inserted into the end of the tube to create an abrupt break in the magnetic field gradient. Figures 2a, b, c show the decoupling field gradient, the Zeeman slower, and velocity distributions before and after slowing, respectively. The magnetic-shield fixture is adjusted at a point near the end of the slower so as to maximize the intensity and minimize the velocity dispersion of the decelerated atoms. Figure 2c shows the velocity dispersion (19 $\mathrm{m\,s^{-1}}$ FWHM) of the cooled atom beam. The abrupt decoupling from $\omega_c$ also prevents optical pumping of the slowed atoms into the $F = 1$ ground state hyperfine level. The atom beam subsequently enters a field-free interaction zone where three light beams labeled $\omega_1, \omega_2, \omega_s$ intersect the atom beam at a common point. The inset in Figure 1 shows the disposition of the atom beam carrying the slowed velocity group and the three light beams. The two beams $\omega_1, \omega_2$ derive from two ring dye lasers (Spectra Physics 380D) and induce photoassociative ionization collisions within the narrow velocity group by the usual two-step process [11]. Figure 3a shows the excitation path leading to PAI. In the first step $\omega_1$, tuned 470 MHz to the red of the Na cycling transition ($I \simeq 600$ $\mathrm{mWcm^{-2}}$), couples incoming atomic scattering flux, entering on the molecular ground state continuum channel, to some bound, long-range attractive molecular state. In a second step $\omega_2$, tuned 700 MHz to the blue of the Na atomic transition ($I \simeq 750$ $\mathrm{mWcm^{-2}}$), couples the bound excited population to an autoionizing doubly excited molecular state. Frequency detunings are relative to the cooled atomic velocity group moving along the atom beam axis at 380 $\mathrm{m\,s^{-1}}$. The inset in Figure 1 shows the angular offset of $\omega_1, \omega_2$ with respect to the atom beam axis (75°, 88°). These offsets angle-tune the two PAI optical beams to excite only the slowed, narrowed velocity group and discriminate against unwanted ionization signals coming from collisions of the background gas or other velocity classes of the sodium jet. The autocorrelation of this laboratory velocity distribution yields the axial collision velocity distribution, and cold collisions with kinetic energy equivalent to a translational temperature of 63 mK take place within the atom beam. A third laser beam, $\omega_s$, derived from the same ring-laser source as $\omega_2$ and tuned $\sim 240$ MHz to the blue of the Na atomic resonance, intersects the atom beam at 90° and provides optical coupling of the incoming flux to an excited repulsive state as shown in Figure 3b. A toothed wheel rotating at 150 Hz chops both $\omega_1$ and $\omega_2$ and provides the external timing signal for a two-channel gated particle counter (Stanford Research Instruments model SR400). Ions are

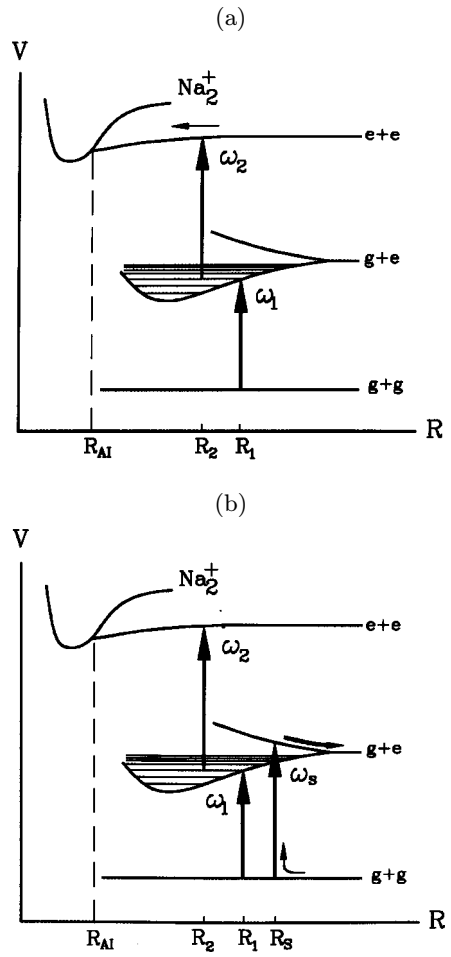


**Fig. 3.** (a) Schematic diagram of the two-step excitation leading to PAI. $R_1 \simeq 520a_0$, $R_2 \simeq 455a_0$, and $R_{AI} = 3a_0$. (b) Suppression of the PAI process by imposition of blue-detuned field with the Condon point $R_s \simeq 650a_0$.

detected on a high-gain CuBe stacked-plate charged-particle detector (Johnston Laboratories model MM1) mounted vertically below the plane containing the optical and atom beams and centered on their intersection point. Channel A counts ions with $\omega_1$ and $\omega_2$ present; channel B counts ions with $\omega_1$ and $\omega_2$ blocked. The PAI signal is the difference between channels A and B. Experimental runs were carried out by measuring the PAI signal with $\omega_s$ present and absent. The ratio of the PAI signal with and without the suppressor beam measures the fractional suppression of the PAI rate. This fractional ratio was recorded as a function of $\omega_s$ intensity and linear polarization, aligned parallel or perpendicular to the atom beam axis. Taking into account detuning, power density, and dwell time in the interaction zone ($\simeq 1$ $\mu$s), we estimate an upper limit to spurious effects due to optical pumping of the Na atoms out of the $F = 2$ ground state hyperfine level by $\omega_s$ to be no more than a few per cent.

Figure 4 shows the relation between the molecular frame scattering angle and the laboratory scattering angle. The two-step PAI mechanism in which the incoming flux is first excited at long range around the Condon point $R_1$,

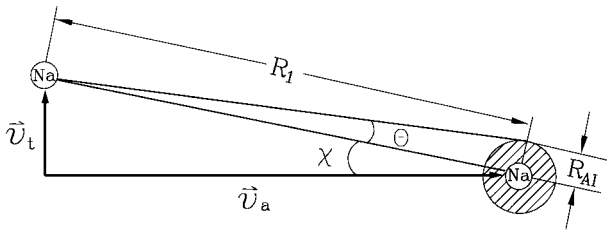


**Fig. 4.** Diagram of the collision angles in the molecular frame and the laboratory frame. With $R_1 \simeq 520a_0$ and $R_{AI} \simeq 3a_0$, the angle $\theta \simeq 6$ mrad. Transverse heating ($v_t \simeq 1.8\ \mathrm{m\,s^{-1}}$) of the axial velocity group ($v_a = 380\ \mathrm{m\,s^{-1}}$) restricts $\chi$ to about 5 mrad.

followed by the autoionizing step at short range $R_{AI}$, narrowly restricts the effective impact parameter or range of scattering angles in the molecular frame. The photoassociating light $\omega_1$ is detuned 470 MHz below atomic resonance which corresponds to $R_1 \simeq 520a_0$. The autoionizing radius at $R_{AI} \simeq 3a_0$ constrains the angular variation $\delta\theta_{col}$ to a narrow cone of about 6 mrad around the internuclear axis in the molecular frame. This angular variation transforms to about $\delta\chi_{col} \simeq 3$ mrad in the *laboratory* reference frame. The molecular collision axis therefore aligns closely along the laboratory axis since the atom beam is collimated in the laboratory system to a divergence of about $\delta\chi_{beam} \simeq 5$ mrad. The polarization axis of the suppressor light $\omega_s$ is of course referenced to the laboratory frame, and the near superposition of the molecular axis (to within several mrad) onto the laboratory atom-beam axis allows us to compare directly measured anisotropy in the laboratory frame to calculated anisotropy in the molecular frame.

## 3 Experimental results and comparison with model calculations

Figure 5 shows a plot of these measurements for two polarization alignments of the suppressor field, $\omega_s$: parallel and perpendicular to the atom beam axis over a range of intensity from zero to about 3 $\mathrm{Wcm^{-2}}$. The error bars ($\pm\sigma$) reflect the uncertainty in the particle counting statistics. In contrast to earlier results [4] which show a marked negative curvature around 2 $\mathrm{Wcm^{-2}}$ suppression intensity, the fractional rate of the PAI process decreases smoothly with increasing suppressor field for both polarizations, decreasing more rapidly for perpendicular alignment than for parallel. Both experimental curves, however, show a less marked suppression effect than that predicted by a two-level, one-dimensional Landau-Zener avoided crossing (1D L-Z) model, shown by the long-dashed line plotted in Figure 5. The figure also compares the experimental results to a three-dimensional version of the Landau-Zener model (3D L-Z). We summarize here essential elements of the Landau-Zener approach in 1D and discuss elaboration to 3D in the next paragraph. In the 1D version, unit scattering flux, or quantum mechanical current $J_S(R_\infty) = 1$, starts at long range on the ground-state entrance channel. At the Condon point $R_s$ where the blue-detuned

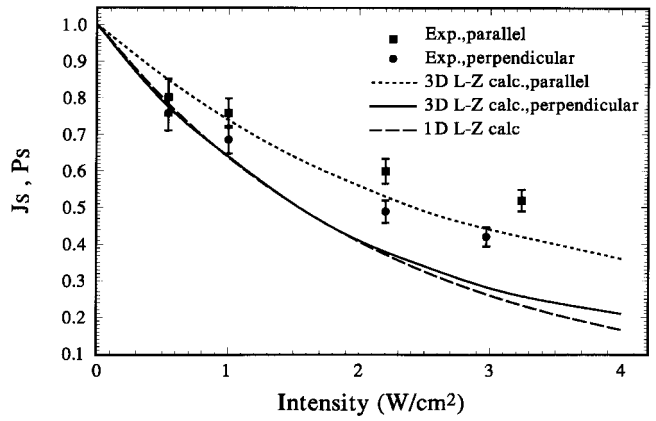


**Fig. 5.** Experimental points showing $P_S$ as a function of $I$, intensity in the suppression laser, $\omega_s$; short-dashed line and solid line are 3D L-Z results of multichannel Landau-Zener calculation by Yurovsky and Ben-Reuven; long-dashed line is 1D L-Z calculation as described in text. The term $J_S$ in the single channel L-Z theory is equivalent to $P_S$ in the multichannel theories.

suppression frequency $\omega_s$ couples resonantly the ground state and the long-range repulsive state, some of the current is deflected onto this repulsive curve and is lost to the PAI process. The L-Z model expresses the "suppressed" probability of PAI as

$$J_S = e^{-A(R_s)} \tag{1}$$

where

$$A(R_s) = \frac{2\pi\hbar\Omega^2}{v(R_s)\left|\left[\frac{d}{R}[\Delta V(R)]\right]_{R_s}\right|} \tag{2}$$

and $\Omega$ is the Rabi frequency of the optical coupling between ground and repulsive states, $v(R_s)$ the local velocity at the crossing point, and $\left|\left[\frac{d}{R}[\Delta V(R)]\right]_{R_s}\right|$ the absolute value of the derivative of the difference potential evaluated at the crossing. The ground state is taken to be flat and the repulsive excited state varies as $C_3/R^3$. The various terms in equation (2) can also be expressed in units convenient for experimental parameters.

$$A(R_s) = \frac{2\pi\Omega^2(\epsilon_f C_3)^{1/3}}{6\sqrt{\epsilon_0\epsilon}\Delta^{4/3}} \tag{3}$$

with $\Omega\,(\mathrm{cm}^{-1}) = 1.71\times10^{-3}\sqrt{I\ (\mathrm{Wcm}^{-2})}$ and $I$ the suppressor laser beam intensity; $C_3 = 6.44e^2a_0^2$ the coefficient of the long-range repulsive curve, $\epsilon\,(\mathrm{cm}^{-1})$ the collision energy at 63 mK, and $\Delta\,(\mathrm{cm}^{-1})$ the blue detuning at $R_s$. The two constants $\epsilon_f = 2.194\times10^5\,\mathrm{cm}^{-1}/\mathrm{au}$, and $\epsilon_0 = \hbar^2/(2\mu a_0^2) = 5.237\ \mathrm{cm}^{-1}$ (with $\mu$ the reduced mass of the colliding partners) are units conversion factors. In both rare gas [5] and alkali MOT experiments [4] as well as in the present atom beam results, the one-dimensional L-Z model seriously overestimates the effect of the suppression at higher fields. Furthermore any 1D theory cannot explain polarization angle differences in the efficiency of shielding or suppression.

Very recently Yurovsky and Ben-Reuven [9] have proposed a multichannel, three-dimensional L-Z approach in which the angular momenta of the collision have been incorporated into the theory. By calculating the L-Z probability at multiple crossings, where incoming $^1\Sigma_g$ ground-state $s$ and $d$ waves couple through $P$, $Q$, $R$ branches to a $^1\Pi_u$ repulsive excited state, various semiclassical pathways are traced out through which the incoming scattering flux can penetrate to the inner region, thereby rendering the shielding less efficient than predicted by the simple 1D L-Z model. Figure 5 shows the results of the Yurovsky–Ben–Reuven model applied to the Na beam experiment [12]. Sodium molecule long-range potentials have been used in these calculations. Unlike the case of the Xe MOT experiments [9], interference terms contributing to the partial-wave scattering amplitude do *not* average to zero for collisions in an atomic beam. For certain choices of the phase in these interference terms, Yurovsky and Ben-Reuven achieve better agreement with the measurements than the conventional one-dimensional, single-crossing L-Z model; and of course they recover the polarization effects. An independent criterion for choosing the phase, however, appears not to be evident.

An alternative to semiclassical L-Z models is to develop a full three-dimensional quantum close coupling calculation of the optical shielding and suppression process which exactly treats the contribution of higher partial-waves to the scattering process as the intensity of the suppression field increases [8]. Although in principle such a theory can take into account the multiplicity of scattering entrance and exit channels generated by fine and hyperfine structure, in practice the computational burden becomes intractable and only calculations of collision rates which ignore nuclear and electron spin can actually be carried out. We have applied this close coupling theory to a model of spinless Na atom collisions subjected to a suppression light field of well-defined intensity $I$, frequency $\omega_s$ and polarization $q$, where we have used realistic scattering potentials [13] for the ground and excited states and the field properties of intensity, detuning and polarization are close to those of the beam experiment. The results of these calculations are compared to the experimental measurements and to the 1D L-Z calculation in Figure 6. In an atom trap, where the distribution of molecular collision axes is isotropic, the rate coefficient $K_{i\to j}$ for the PAI channel $j$ starting from the entrance ground state channel $i$ is given by

$$\begin{aligned} K_{i\to j} &= \frac{v_{rel}}{4\pi}\int_0^{\pi}\sin\theta_{\mathbf{k}}d\theta_{\mathbf{k}_i}\int_0^{2\pi}d\varphi_{\mathbf{k}_i}\int_0^{\pi}\sin\theta\,d\theta \\ &\quad\times\int_0^{2\pi}d\varphi\left|f_i^j(\theta_{\mathbf{k}_i},\varphi_{\mathbf{k}_i},\theta,\varphi)\right|^2 \\ &= v_{rel}\frac{\pi}{\mathbf{k}_i^2}\sum_{l=0}^{\infty}\sum_{m_l=-l}^{+l}\sum_{l'=0}^{\infty}\sum_{m_l'=-l'}^{+l'}\left|T_{i,l,m_l}^{j,l',m_l'}\right|^2 \end{aligned} \tag{4}$$

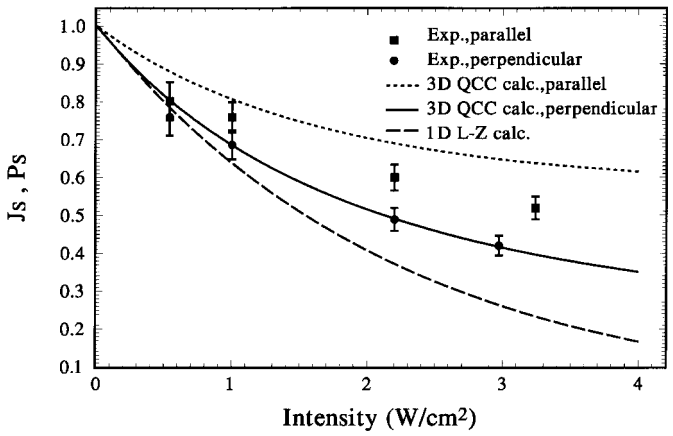


**Fig. 6.** Experimental results showing the fractional suppression of PAI (equivalent to the shielding measure, $P_S$) for $\omega_s$ linearly polarized parallel and perpendicular to the atom beam axis as a function of the intensity in the suppressor laser beam. Also shown are results from a quantum close-coupling calculation (QCC) of the shielding measure $P_S$ and the probability of penetration $J_S$ for the 1D L-Z theory. The term $J_S$ in the single channel L-Z theory is analogous to $P_S$ in the multichannel theories.

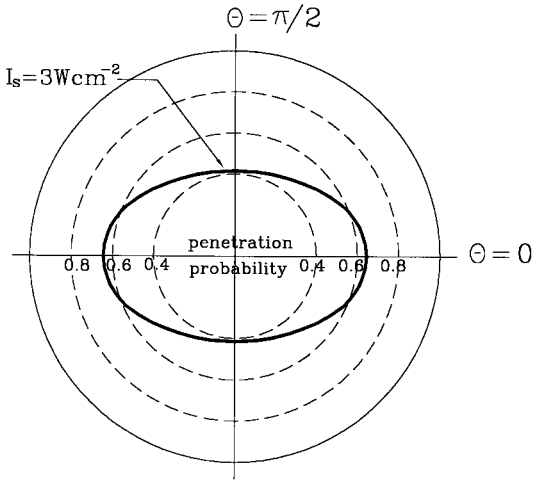


**Fig. 7.** Polar plot of the calculated penetration probability or shielding measure $P_S$. The plot is calculated using the parameters of the present experiment.

where $v_{rel}$ is the relative collision velocity, $f_i^j(\theta_{\mathbf{k}_i}, \varphi_{\mathbf{k}_i}, \theta, \varphi)$ the scattering amplitude, $\theta_{\mathbf{k}_i}, \varphi_{\mathbf{k}_i}$ specify the incident direction, and the rate is averaged over initial angles and summed over final angles. The second line of equation (4) derives from the expression of the scattering amplitude in terms of the $T$ matrix between initial state $i$ with partial wave $l, m_l$ and final state $j$ with partial wave $l', m_{l'}$. In a beam experiment, however, the initial collision-axis angles are narrowly restricted, and if equation (4) is only integrated over the final directions, the result is

$$K_{i\to j} = v_{rel}\frac{4\pi^2}{\mathbf{k}_i^2}\sum_{l'=0}^{\infty}\sum_{m_{l'}=-l'}^{l'}\left|\sum_{l=0}^{\infty}\sum_{m_l=-l}^{+l} \times Y_l^{m_l^*}(\theta_{\mathbf{k}}, \varphi_{\mathbf{k}}) i^l T_{i,l,m_l}^{j,l',m_l'}\right|^2. \quad (5)$$

The key difference between equation (4) and equation (5) is the retention of the $Y_l^{m_l^*}(\theta_{\mathbf{k}}, \varphi_{\mathbf{k}})$ spherical harmonic factor that provides the angular modulation of the $K_{i\to j}$ rate expression. At low suppressor intensity only the lowest $l$ wave (the $s$ wave for identical bosons) will contribute to the sum in equation (5), and the rate will be isotropic. But as the $\omega_s$ intensity increases, the light field will couple higher $l$ wave terms in the $T$ matrix, and the angular dependence of these higher $l$ waves will strongly modulate the angular dependence of the $K_{i\to j}$. At 63 mK collision energy, the centrifugal potential barrier height will prevent more than three partial waves $(s, d, g)$ from contributing to the sum; and the predicted anisotropy of the "shielding measure" $P_S(I, \theta_{\mathbf{k}}, \varphi_{\mathbf{k}})$ as a function of $\theta$, the angle between the collision axis and $\omega_s$ linear polarization axis is shown in Figure 7. The definition of the shielding measure is

$$P_S(I, \theta_{\mathbf{k}}, \varphi_{\mathbf{k}}) = \frac{\sigma_{i\to j}(I, \theta_{\mathbf{k}}, \varphi_{\mathbf{k}})}{\sigma_{i\to j}\,(I=0)} \quad (6)$$

where $\sigma_{i\to j}(I, \theta_{\mathbf{k}}, \varphi_{\mathbf{k}})v_{rel} = K_{i\to j}$. At these low collision temperatures velocity averaging over the thermal distribution is negligible, and equation (6) can be associated with the ratio of the PAI rate constant in the presence and absence of the $\omega_s$ suppressor light. The calculated shielding measures $P_S(I, \theta_{\mathbf{k}} = 0)$ and $P_S(I, \theta_{\mathbf{k}} = \pi/2)$ provide the point where theory and experiment meet, and they can be compared to the measured ratios of the PAI rate with the suppression light polarized parallel and perpendicular to the beam axis as a function of increasing $\omega_s$ intensity in Figures 6 and 5.

## 4 Discussion

It is clear that both the multichannel L-Z theory of Yurovsky and Ben-Reuven [9] and the quantum close coupling model of Napolitano *et al.* [8] reproduce the general dependence of the suppression effect on $\omega_s$ intensity and the relative ordering of $\omega_s$ polarization. How can one compare and contrast these two approaches? The multichannel L-Z approach is semiclassical in the sense that scattering flux is pictured to move along well-defined potentials, jumping between them with L-Z probabilities calculated at the crossing points. These crossing points are coupled by the optical dipole interaction of the suppressor field. But this approach is quantum in the sense that the scattering flux resolves into contributing partial waves, and the total probability of penetration into the inner region must take account of all the possible routes of partial wave propagation. Figure 8 presents a schematic network of potentials tracing the pathways through which the scattering flux can penetrate to the

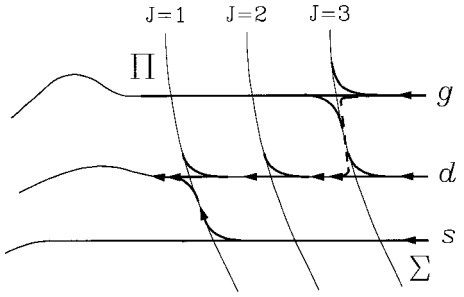


**Fig. 8.** Schematic of the multichannel L-Z model. Rotational motion of the two atoms colliding on a flat ground $\Sigma$ state and optically coupled to a repulsive $\Pi$ state is represented by a network of intersecting partial wave potentials. Landau-Zener probabilities are evaluated at each crossing, and the overall probability of penetration is constructed from the crossings along various pathways. "Intuitive" pathways are shown as solid lines and a "counterintuitive" pathway is shown as a dashed line. The family of repulsive curves are labeled by the total angular momentum $J$ of the collision system, including the angular momentum of orbital motion and the resultant internal angular momentum from each atom.

inner region where PAI takes place. When flux entering on several partial waves converges and penetrates to the inner region along the same potential, interference terms will appear in the calculation of the shielding measure. For certain choices of the phase angle in these interference terms Yurovsky and Ben-Reuven [12] obtain good agreement with the experimental results reported here, but the justification for these choices remains unclear. Furthermore not all pathways have been included in the model. In particular the "counterintuitive" pathways on which the incoming flux makes a sharp "hairpin" turn, moves backward for an interval before undergoing another sharp turn at the next crossing, have not been included. The counterintuitive pathways lead to penetration along lower angular momentum barriers and should therefore become relatively more important as the collision temperature reduces. In contrast the quantum close coupling approach makes no attempt to trace the paths of collisional intermediate states, but numerically solves the Schroedinger equation for initial scattering boundary conditions, well-defined potentials, and optical coupling. As fewer partial waves contribute to the scattering process, the amplitude and anisotropy of the shielding measure calculated by these two approaches may distinguish them. One might expect that the multichannel L-Z approach without the "counterintuitive" pathways would predict a smaller suppression effect as temperature decreases than does the quantum close coupling theory which makes no distinction between intuitive and counterintuitive channels. Further development of both models may be needed however before an experiment can be designed to test their predictions.

In summary we have measured the polarization anisotropy of optical suppression in photoassociative ionization collisions within a highly collimated and cooled Na atomic beam as a function of the suppressor-field intensity. We have compared these measurements to the results of three model calculations of the suppression process: a simple single-channel 1D L-Z model, a multichannel 3D L-Z theory, and a quantum close-coupling (QCC) approach. Both the semiclassical 3D L-Z picture and the close-coupling calculations give reasonable agreement with the experimental results, but both models ignore the effects of electron and nuclear spin on the molecular states of the colliding atom pair. Measurements at lower temperature, which exclude a greater number of partial waves from the scattering amplitude, may reveal differences in the predictions of the semiclassical and quantum calculations, and yield better insight into the nature of the suppression process itself.

## References

1. J. Weiner, V.S. Bagnato, S. Zilio, P.S. Julienne, Rev. Mod. Phys. (in press, 1998).
2. L. Marcassa, S. Muniz, E. de Queiroz, S. Zilio, V. Bagnato, J. Weiner, P.S. Julienne, K.-A. Suominen, Phys. Rev. Lett. **61**, 935 (1994).
3. L. Marcassa, R. Horowicz, S. Zilio, V. Bagnato, J. Weiner, Phys. Rev. A **52**, R913 (1995).
4. S.C. Zilio, L. Marcassa, S. Muniz, R. Horowicz, V. Bagnato, R. Napolitano, J. Weiner, P.S. Julienne, Phys. Rev. Lett. **76**, 2033 (1996).
5. M. Walhout, U. Sterr, C. Orzel, M. Hoogerland, S.L. Rolston, Phys. Rev. Lett. **74**, 506 (1995).
6. H. Katori, F. Shimizu, Phys. Rev. Lett. **73**, 2555 (1994).
7. K.-A. Suominen, K. Burnett, P.S. Julienne, M. Walhout, U. Sterr, C. Orzel, M. Hoogerland, S.L. Rolston, Phys. Rev. A **53**, 1658 (1996).
8. R. Napolitano, J. Weiner, P.S. Julienne, Phys. Rev. A **55**, 1191 (1997).
9. V.A. Yurovsky, A. Ben-Reuven, Phys. Rev. A **55**, 3772 (1997).
10. W.D. Phillips, J.V. Prodan, H.J. Metcalf, J. Opt. Soc. Am. B **2**, 1751 (1985).
11. P.S. Julienne, R. Heather, Phys. Rev. Lett. **67**, 2135 (1991).
12. V.A. Yurovsky, A. Ben-Reuven (unpublished).
13. H.R. Thorsheim, J. Weiner, P.S. Julienne, Phys. Rev. Lett. **58**, 2420 (1987).